

# Addressing the Non-perturbative Regime of the Quantum Anharmonic Oscillator by Physics-Informed Neural Networks

Lorenzo Brevi,<sup>1</sup> Antonio Mandarino,<sup>1</sup> and Enrico Prati<sup>1,\*</sup>

<sup>1</sup>*Department of Physics Aldo Pontremoli, Università degli Studi di Milano, Via Celoria 16, 20133 Milano, Italy*  
(Dated: May 24, 2024)

The use of deep learning in physical sciences has recently boosted the ability of researcher to tackle physical systems where little or no analytical insight is available. Recently, the Physics-Informed Neural Networks (PINNs) have been introduced as one of the most promising tools to solve systems of differential equations guided by some physically grounded constraints. In the quantum realm, such approach paves the way to a novel approach to solve the Schrödinger equation for non-integrable systems. By following an unsupervised learning approach, we apply the PINNs to the anharmonic oscillator in which an interaction term proportional to the fourth power of the position coordinate is present. We compute the eigenenergies and the corresponding eigenfunctions while varying the weight of the quartic interaction. We bridge our solutions to the regime where both the perturbative and the strong coupling theory work, including the pure quartic oscillator. We investigate systems with real and imaginary frequency, laying the foundation for novel numerical methods to tackle problems emerging in quantum field theory.

## I. INTRODUCTION

Much of the modern understanding in physics is due to the theoretical framework posed in place by quantum field theories. Ranging from the quantization of the electromagnetic field to the explanation of heat conduction in solids, the ingenious and *revolutionary trick* was to rethink the fields as a collection of harmonic oscillators [1]. Since harmonic systems are one of the few integrable systems either in classical or quantum mechanics, and even if the solution of harmonic systems is an academic exercise, it is also wide knowledge how predictive these systems are. This implies that analytical computations allow the knowledge of their entire spectrum and to gain insight from a multitude of physical systems thanks to the mapping between bosonic systems and the quantum harmonic oscillator [2]. This boosted not only the acclaimed achievements in the quantum theory of radiation [3, 4], but also the application of field theoretical tools to treat the small oscillations in molecules [5] or in the solid lattice and fostered our understanding of condensed matter. [6].

However, if the harmonic potential is modified by the addition of terms proportional to higher powers of the position coordinates, the system loses almost always its integrability <sup>1</sup> [7]. Nevertheless, since the pioneering work by lord Rayleigh in classical physics [8] and subsequently by Schrödinger [9] in the quantum context, it was shown that slight perturbation breaking the harmonicity can be successfully treated within the framework of perturbation theory. In the present paper, we aim to provide a deep-learning perspective on a system that has long

served as a prototypical interaction model [10, 11], and it served and still serves to study innovative techniques in quantum field theory [12–16]. The anharmonic oscillator with a term proportional to  $x^4$  can be indeed seen as a  $\lambda\phi^4$  theory in  $(0+1)$ -dimensions. Furthermore, such a system has been consistently used in several contexts, most notably in solid-state physics to account for the hardening of the phonon dispersion relation [17–19], to investigate the formation of molecules with hydrogen bonds and their vibrational modes [20, 21], but also for foundational studies such as nonlinear quantum mechanics [22, 23], quantum chaos and control [24, 25].

Some of us have already developed both supervised [26–28] and unsupervised [29] machine learning methods, including supervised quantum machine learning to address ground state classification [30–32] of a physical system. Here, we aim to address the unsupervised solution of the Schrödinger [33] equation, to explore the potential of Physics-Informed Neural Networks (PINNs) for solving Partial Differential Equations (PDEs) as a paramount representative application to nontrivial physical phenomena.

We applied the method to find both the ground state and the excited states of the quantum harmonic and anharmonic oscillator, with real or imaginary frequency. We employed a PINN that splits into two separate networks [34], one for the eigenvalue and one for the eigenfunction. Furthermore, it also employs an auxiliary output [35] to obtain the normalization integral. We also employed transfer learning, utilizing the weights and biases of the already trained networks to obtain an excellent initialization for networks with similar parameters.

The remaining part of the paper is organized as follows. In Section II, we briefly introduce the details of the deep learning model employed, explaining in particular loss functions and architecture of the neural network. Section III gives the detail of the quantum anharmonic oscillator, and delves into the detailed explanation of the unsupervised learning strategy that we followed. Section

\* enrico.prati@unimi.it

<sup>1</sup> It is worth noting that the Morse potential (and several of its variations) can account for the anharmonic behavior and are still integrable.

IV shows the results for the unperturbed (harmonic) oscillator while in Section V the results for the anharmonic oscillator are described. Section VI shows the results for the pure quartic oscillator while in Section VII we address the scaling behavior of the eigenenergies in function of  $\lambda$ . Lastly, Section VIII concludes the paper and address some interesting perspectives for future research directions.

## II. BACKGROUND

This sections contain in a concise form the required background information for our analysis. We start with a brief introduction to the considered neural network architecture, afterward we discuss the relevance of the considered model, especially from a field theory point of view.

### A. Physics-informed neural networks

Physics-informed neural networks [36], or PINNs are a category of neural networks that aim to solve Partial Differential Equations by encoding prior knowledge about the physical system, most importantly the differential equation itself, in their loss function. This loss can be written as:

$$f = MSE_{PDE} + MSE_{data} + MSE_{phys} \quad (1)$$

Where  $MSE_{data}$  is the standard loss for a Neural Network <sup>2</sup>.  $MSE_{phys}$  corresponds to the losses given by the physical constraints of the system, like boundary conditions and initial conditions. Lastly,  $MSE_{PDE}$  is the mean squared error of the differential equation. For instance, given a PDE with implicit solution  $\mu(t)$  that depends on  $\mu(t)$  and its derivative  $\partial_t \mu(t)$  with respect to the independent variable  $t$ , the differential equation can be written as:

$$\partial_t \mu(t) + N[\mu; \lambda] = 0 \quad (2)$$

where  $N$  is a nonlinear operator and  $\lambda$  is some set of parameters. Given this, we can write  $MSE_{PDE}$  for a network designed to solve this equation as:

$$\frac{1}{n} \sum_{i=1}^n (\partial_t \mu(t_i) + N[\mu(t_i); \lambda])^2 \quad (3)$$

Where the  $t_i$  is the set of  $n$  points, called collocation points, where the PDE will be evaluated. This makes it possible to train neural networks even in the presence

of noisy or very little data, and even in a fully unsupervised setting, such as in this paper. These networks have had a number of applications in various fields. Just to name a few applications of PINNs, the most recent and relevant use cases are in fluid dynamics [37–39], heat transfer problems [40], scattering in composite optical materials [41], oscillating dynamics of black holes ([42]), reconstruction of top quark kinematic properties ([43]) and to compute the electronic density in complex molecular systems ([44]).

### B. The quantum anharmonic oscillator

The anharmonic oscillator model has played a pivotal role in many research areas in physics, mostly due to its simplicity but especially because it is a nontrivial nonlinear problem. It appeared to be crucial in the development of several branches of physics ranging from high-energy particle physics to low-energy molecular dynamics. The Hamiltonian describing the problem in one-dimension for a system of unitary mass is:

$$H = \frac{p^2}{2} + V(x) = \frac{p^2}{2} + \frac{\omega^2 x^2}{2} + \lambda x^4 \quad (4)$$

in which  $\omega$  is the harmonic frequency and  $\lambda$  quantifies the strength of the interaction-like term, and finally  $p$  and  $x$  are the standard position and momentum operator satisfying  $[x, p] = i$ . The potential  $V(x)$  could assume two relevant shapes for physical applications, depending on the signs of  $\omega^2$  and  $\omega^2/\lambda$ . When both terms are positive the potential has only one minimum and its shape is that of a “super parabola”, whereas when the frequency is imaginary, we are in the presence of a double-well potential that is the archetype of a model exhibiting a spontaneously symmetry-breaking mechanism. Without losing generality in the following we will assume that the oscillator has unitary mass and we will work in natural units  $m = c = \hbar = 1$ , where  $m$  is the mass of the oscillator,  $c$  and  $\hbar$  are the speed of light in the vacuum and the reduced Planck constant respectively.

Since the preliminary works of Bender and Wu [10–12] based on perturbative expansions in  $\lambda$ , several techniques have been deployed to study the spectrum of this Hamiltonian. A notable observation noted by Bender and Wu, employing the Wentzel–Kramers–Brillouin approximation, was that for any  $\lambda \neq 0$  the perturbative series is divergent. Later on Zinn-Justin and collaborators proposed perturbative solutions in terms of instantons connecting the two minima of potentials characterized by  $\omega^2 < 0$ , which are particularly suitable for weakly interacting scalar fields exhibiting spontaneously broken symmetries [45–48]. More recently, the Schrödinger equation stemming from the Hamiltonian in Eq. (4) was mapped in a Riccati form and some approximated eigenfunctions were obtained in [7, 49].

<sup>2</sup> In our case this loss will not be present since we are working in an unsupervised setting

### III. METHODOLOGY

To obtain eigenfunctions and eigenstates for the anharmonic oscillator, we employ two neural networks that will be trained in parallel. Both networks take the same input, the position  $x$ , which will be sampled in an interval  $[-\frac{L}{2}, \frac{L}{2}]$  where  $L$  is a hyperparameter that controls the size of the computational domain and has to be chosen large enough that the wave function is vanishingly small at the system's boundary, but not so large that the network has to predict a vast area of just zeros. The first neural network will output the wave function  $\psi(x)$  and the auxiliary output  $\nu(x)$ , which is defined as:

$$\nu(x) = \int_{-\frac{L}{2}}^x |\psi(k)|^2 dk \quad (5)$$

and will be used to ensure normalization. On the other hand, the second network will output a vector of guesses for the energy. We take as the actual guess for the eigenvalue the average of the outputs of the second Neural Network.

We need to optimize a total of 7 losses to train the network. First of all, we need a way to compute the integral of the square module of the eigenfunction to be able to normalize the wave function. To do it in a mesh-free way we utilize an auxiliary output,  $\nu(x)$ , and train the network to make it a guess for integral from 0 to  $x$  of the square module of the outputted wave function, (see equation (5)). To ensure that this auxiliary output has the desired form, we utilize automatic differentiation to obtain the partial derivative of the auxiliary output, and require it to be equal to the squared modulus of the wave function, thus obtaining the integral loss:

$$\left. \frac{\partial \nu(x')}{\partial x'} \right|_{x'=x} = |\psi(x)|^2, \quad (6)$$

where the partial derivative of the auxiliary output can easily be obtained thanks to automatic differentiation. Of course, if this loss is satisfied then the auxiliary output will have the desired form (5). At this point, we need to ensure that the output of the network respects the physical constraints of the system. This is accomplished through three more losses. The first is the normalization loss:

$$\nu(-\frac{L}{2}) = 0, \quad \nu(\frac{L}{2}) = 1. \quad (7)$$

which ensures that the wave function is normalized. Furthermore, and maybe more importantly, this loss forces the neural network to actually predict the eigenfunctions instead of just a constant stream of zeros, since it is the only loss to not be exactly satisfied when  $\psi(x) = 0$  for all  $x$ .

We then utilize the boundary condition loss:

$$\psi(-\frac{L}{2}) = 0, \quad \psi(\frac{L}{2}) = 0 \quad (8)$$

to ensure that the wavefunction is vanishingly small at the borders of the domain. The last physical constraint to encode as a loss is the orthogonality of the eigenstates, which will allow the PINN to also find the excited states by imposing for the state predicted by the current network to be orthogonal to all previously found states. This can be accomplished by the orthogonality loss:

$$\sum_i \langle \psi(x) | \psi_i(x) \rangle = 0 \quad (9)$$

where  $\psi_i(x)$  are the known eigenfunctions. This loss will always be 0 when training the first network, the one that will be trained to output the ground state, but each time a network converges it will be saved and utilized to obtain the  $\psi_i(x)$  utilized to compute this loss in the training of the networks of higher energy states. At this point, we need to include the loss that will allow the network to gauge the correctness of the outputted eigenstate and eigenvalue for the current potential, that is the differential equation loss:

$$-\frac{1}{2} \frac{\partial^2 \psi(x)}{\partial x^2} + (\frac{1}{2} \omega^2 x^2 + \lambda x^4) \psi(x) - E \psi(x) = 0 \quad (10)$$

which is just the Schrödinger equation that stems from the Hamiltonian in Eq. (4). At this point, we have a set of losses that will result in a neural network that will output one of the eigenstates for the given potential. However, we have no guarantee that this state is the one with the lowest energy among the ones that have not yet been discovered. To ensure this we need to add a condition that forces the network to minimize the energy. We use:

$$e^{a(E_{PINN} - E_{init})} = 0, \quad (11)$$

where  $E_{PINN}$  is the predicted energy,  $a$  is a hyperparameter, and  $E_{init}$  is either another hyperparameter, when  $n = 0$ , or the energy of the previous state, for excited states. The choice to increase  $E_{init}$  as the quantum number increases has been taken to avoid an excessive weight for this loss for a higher energy state, which might cause the network to fail to converge at all. The energy minimization loss, however, will be greater than 0 even when we reach the correct solution, and that will cause the network to converge to an incorrect state. In order to avoid this we gradually decrease this loss' weight as the training continues. In this way in the earlier epochs, this loss will steer the network towards lower energy states, while for the latter epochs it will become negligible and allow the network to settle to the correct solution.

The last loss that we implement is one that is not actually needed to obtain a solution, but is instead added to allow the network to converge much faster, acting as an inductive bias: the symmetry loss. Since the potential is symmetric with respect to 0, the wave functions that solve Eq. (10) will also have to be alternatively symmetric and anti-symmetric with respect to 0. We can enforce this condition by adding the loss:

$$\psi(x) - s\psi(-x) = 0 \quad (12)$$

where  $s$  is a parameter that assumes the value one if we are looking for a symmetric state ( $n$  even), or  $s = -1$  if we are looking for an anti-symmetric one ( $n$  odd). For the sake of clarity, it is worth mentioning that the value of  $s$  starts at one and is switched every time a new model is trained.

For the architecture, the network that outputs the wave function and the integral is made up of 7 hidden layers of 256 neurons each while the one used to predict the energy is made up of 4 layers, also of 256 neurons. Batches of 512 collocation points were employed. We want each batch to span the whole domain, but we also want to utilize fully the mesh-free nature of the neural method. To do so we construct a grid of 512 equally spaced points, and for each of them, we sample randomly in an interval centered on it, thus obtaining a batch that spans the whole domain but whose values change slightly at each iteration, ideal characteristics to optimize the network's convergence.

### A. Weights

To allow the training to converge, we need to set the correct weights for each of the losses. Empirically, it seems that the most effective weights give each of the losses a scale, causing the network to try to reduce them in order. In particular, the chosen weights are such that the model is first forced to enforce the physical constraints of the system, such as the normalization, and only afterward it will start to try to minimize the differential equation loss. We obtain the results reported below in Table I:

Loss	Weight
Normalization	500
Integral	1000
Boundary conditions	10
Symmetry	1000
Orthogonality	500 n
Differential equation (starting)	1
Energy minimization (starting)	100

TABLE I: Weights for the different losses

This choice of weights ensures that first of all the network learns how to compute the integral. Once it has learned how to, it can use this integral to enforce normalization, which must be the first thing the network learns so that it does not just predict constant zeros and get stuck in a local minimum. After that, it will enforce the boundary and orthogonality conditions. Furthermore, the differential equation's weight is linearly increased to ensure that the solution of the actual equation takes priority in later epochs. The symmetry loss weight has been set so high in order to guarantee that it limits the possible solutions accepted by the network and thus accelerates convergence.

The Orthogonality loss is proportional to the quantum number of the excited state we want to study.

### B. Evaluation metrics

When the exact solutions are known, the solution given by the trained network is evaluated by utilizing two metrics. To gauge the eigenvalue's correctness we utilize the relative error for the energy:

$$err_E = \frac{E_{Ex} - E_{PINN}}{E_{Ex}}, \quad (13)$$

where  $E_{Ex}$  is the analytic value of the energy, while  $E_{PINN}$  is the one predicted by the network. On the other hand to evaluate the eigenvector the fidelity between the predicted wave function and the exact one [50–52] is employed:

$$\mathcal{F}_\psi = |\langle \psi_{Ex} | \psi_{PINN} \rangle|^2, \quad (14)$$

numerically evaluated as:

$$\mathcal{F}_\psi = \left| \sum_i \psi_{PINN}(x_i) \overline{\psi_{Ex}(x_i)} \right|^2 \quad (15)$$

where the  $x_i$  are a set of points spanning the whole domain, and  $\psi_{Ex}(x)$  and  $\psi_{PINN}(x)$  are the values of the wave function at the point  $x$  as given by the analytic expression and by the network, respectively. Both of the vectors will be normalized before calculating the similarity, to avoid getting incorrect results due to inaccurate scaling. This should equal one when the two wave functions are the same. These metrics, however, might depend on the choice of evaluation points. Therefore once the training has converged we compute them 1000 times for different sets of points, sampled in the same way we sample the training batches, to make sure that we always get a different set of points, and that each of these sets still spans the whole domain, to obtain a valid estimate of the fidelity. The final values will be the average of these estimates and will come with a standard deviation quantifying the dependence on the choice of evaluation points. For a deeper analysis, in which we discuss better the variance of these results we refer the reader to Section VII.

### C. Choice of the domain

We need to choose an  $L$  such that the wave function is vanishingly small at the boundaries, but at the same time,  $L$  should be as small as possible to avoid training the network on areas of just 0s, which would make the network vastly underestimate the orthogonality loss (9) when using Mean Squared Error. This means that the optimal choice of  $L$  depends on the state that we want to train the network to predict, since for this type of potential higher energy states will tend to be less localized

and we must therefore choose a domain that grows as  $n$  increases<sup>3</sup>. In particular, we empirically find that a good value for  $L$  for the unperturbed oscillator is:

$$L(n) = 7 + 2n \quad (16)$$

However, the potential of the anharmonic oscillator will grow faster than the purely harmonic one. Therefore, the resulting wave functions will be more localized, meaning that it will be better to train the network in a smaller domain. In particular, a good starting point is the interval  $[-\frac{L_a}{2}, \frac{L_a}{2}]$  such that  $V_{ANH}(\frac{L_a}{2}) = V_H(\frac{L}{2})$ , where  $V_{ANH}$  is the anharmonic potential  $\frac{1}{2}\omega^2 x^2 + \lambda x^4$  and  $V_H$  is the harmonic potential  $\frac{1}{2}\omega^2 x^2$ . Thus, given  $n$  and  $\lambda$ ,  $L_a$  will be the solution to:

$$\lambda(\frac{L_a(n, \lambda)}{2})^4 + \omega(\frac{L_a(n, \lambda)}{2})^2 = \omega(\frac{L(n)}{2})^2 \quad (17)$$

To that we add a constant  $\epsilon = 1$  on each side of the interval to ensure some leeway<sup>4</sup>, thus obtaining:

$$L_a = 2 \left( \sqrt{\frac{-1 + \sqrt{1 + 4\frac{\lambda}{\omega}(\frac{L}{2})^2}}{2\frac{\lambda}{\omega}}} + \epsilon \right) \quad (18)$$

#### IV. RESULTS FOR THE HARMONIC OSCILLATOR

We train the network to predict the first six stationary states. The training is stopped as soon as the total loss becomes less than 0.1 and the differential equation loss is smaller than  $3 \times 10^{-3}$ , in order to obtain good guesses for the energies and eigenstates without requiring an overly long computational time. We set  $E_{init} = 0$  and  $a = 0.8$  in (11), and obtain the values reported below in Table II:

$n$	$err_E$	$\mathcal{F}_\psi$
0	$7.45 \times 10^{-4} \pm 10^{-5}$	$0.9999926 \pm 2.38 \times 10^{-10}$
1	$-2.79 \times 10^{-3} \pm 8.18 \times 10^{-6}$	$0.9999751 \pm 3.20 \times 10^{-10}$
2	$-4.87 \times 10^{-3} \pm 1.25 \times 10^{-5}$	$0.9998467 \pm 2.64 \times 10^{-9}$
3	$-6.70 \times 10^{-3} \pm 9.79 \times 10^{-6}$	$0.9997815 \pm 3.61 \times 10^{-9}$
4	$-6.05 \times 10^{-3} \pm 7.21 \times 10^{-6}$	$0.9997674 \pm 4.19 \times 10^{-9}$
5	$-8.30 \times 10^{-3} \pm 1.16 \times 10^{-5}$	$0.9997969 \pm 3.79 \times 10^{-9}$

TABLE II: Results for the error and the fidelity between the exact state and the state computed by the neural network for the harmonic unperturbed oscillator.

<sup>3</sup> If this means that we need to extrapolate, for instance when obtaining the values of  $\psi_i(x)$  for the orthogonality loss, we just predict 0 outside the original computational domain since the wave function should be negligible outside it.

<sup>4</sup> But if this makes  $L_a(n, \lambda) > L(n)$ , we just use  $L(n)$

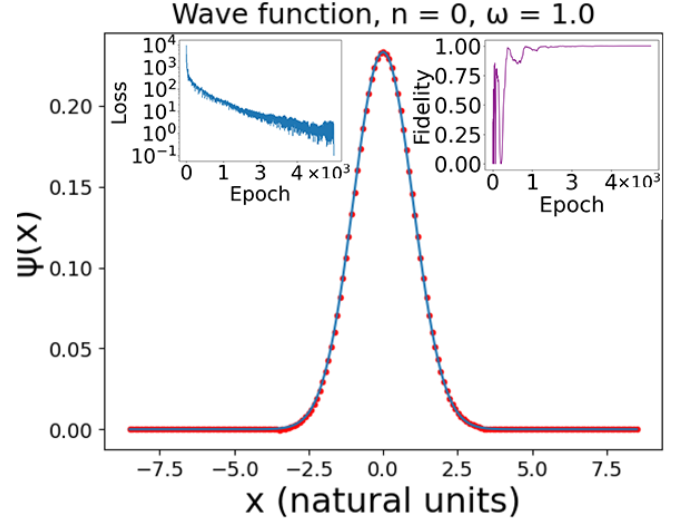


FIG. 1: Final wave function for the ground state. The blue line is the analytic wave function, while the red dots are the neural network prediction. In the left inset (in blue): the behavior of the loss throughout training, in logarithmic scale. In the right inset (in purple): fidelity throughout training

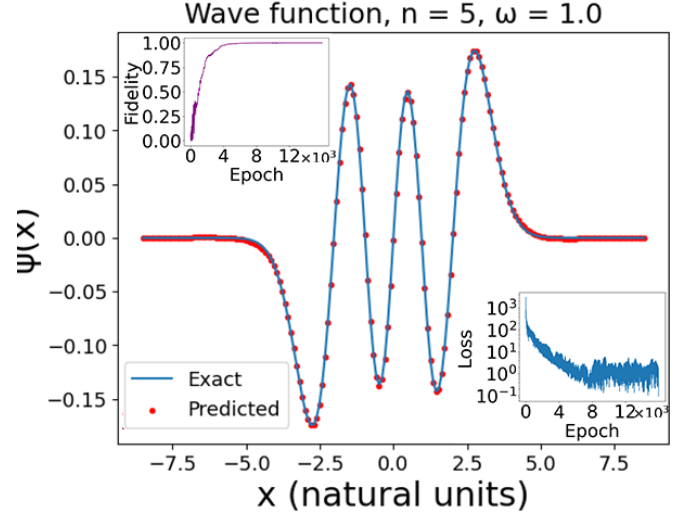


FIG. 2: Final wave function for the fifth excited state. The blue line is the analytic wave function, while the red dots are the neural network prediction. In the inset: the behavior of the loss throughout training, in logarithmic scale. In the right inset (in purple): fidelity throughout training

The error on the eigenenergy always stays beneath the 1%. The results for the fidelity are also more than acceptable, with a distance of at most in the order of  $10^{-4}$ , even though the fidelity slightly decreases as the energy increases. Some examples of the final results and the behavior of the loss and fidelity throughout the training process are reported in Figure 1 for the ground state,

and in Figure 2 for the fifth excited state. In particular, looking at the behavior of the loss we can see it is mostly monotonically decreasing, but for  $n = 5$  it takes roughly double the epochs then  $n = 0$  to get to the same value. Still, it shows good convergence. Concerning fidelity, it displays excellent behavior for  $n = 5$ , asymptotically approaching 1. On the other hand, the behavior for  $n = 0$  is more complex. It rapidly approaches 0.8, then goes back down to almost 0, and eventually rises up until it reaches 1. A possible explanation could be that the network was approaching the ground state, then it risked converging to an excited state, which will be orthogonal to the ground and therefore with fidelity zero, but after several epochs it managed to converge to the correct state, thanks to the energy minimization condition.

## V. SPECTRUM OF THE ANHARMONIC OSCILLATOR

In this section, we report the main results of this paper. As introduced in Section II both the cases of real and imaginary frequency are analyzed.

### A. Oscillator with real frequency

We now add the quartic potential to the oscillator. In particular, we will use  $\omega = 1$  and train the neural network with  $\lambda = 0.005 \times 2^n$ , with  $n$  from 0 to 12. These choices of  $\lambda$  will allow us to study cases in which the quartic potential is just a perturbation, in which the two potentials have the same scales and in which the quartic part is dominant, up until the point where the system is basically just a pure quartic oscillator. In order to guarantee convergence, we exploit the results of section (IV) and employ transfer learning: we initialize the weight of the network to the ones that give the eigenfunction and eigenvalue of the harmonic oscillator, thus ensuring that the network starts close to the minima. Then, as  $\lambda$  increases, we always initialize the network to the weight and biases as the already solved one with the closest  $\lambda$ . Due to this initialization, it becomes less important to enforce the orthogonality and energy minimization losses, since the minima closer to the starting state should already be the one corresponding to the correct eigenstate and eigenenergy, which means that we do not need these two losses as much to drive the network away from unwanted minima. Therefore, their starting weights have been decreased to  $100n$  and  $0.1$  respectively. The network manages to reach the convergence conditions for all values of  $\lambda$  and  $n$ . Thanks to transfer learning, these results were also reached much quicker (5 to 10 minutes for lower excited states, compared to 20 to 40 minutes when given a clean initialization).

At this point we compare the obtained eigenenergies with those one gets from the standard perturbation the-

n	$\lambda$	$(E_{pert} - E_{PINN})/E_{pert}$
0	0.005	$2.06 \times 10^{-2} \pm 2.47 \times 10^{-5}$
5	0.005	$-8.67 \times 10^{-4} \pm 5.18 \times 10^{-7}$
2	0.16	$1.56 \times 10^{-2} \pm 1.27 \times 10^{-5}$
2	0.32	$-1.87 \times 10^{-3} \pm 8.34 \times 10^{-6}$
2	0.64	$-4.79 \times 10^{-2} \pm 8.04 \times 10^{-6}$
3	1.28	$-2.41 \times 10^{-1} \pm 3.16 \times 10^{-6}$
0	10.24	$-4.18 \times 10^{-1} \pm 1.03 \times 10^{-5}$
5	10.24	$-7.94 \times 10^{-1} \pm 6.21 \times 10^{-6}$

TABLE III: Some results for the anharmonic oscillator. We can clearly see how for low  $\lambda$  the energy predicted in perturbation theory and the one predicted by the neural network agree, but differ substantially from  $\lambda$ s comparable to or higher than  $\omega$

ory. In particular, we will have, for  $\omega = 1$  [53]:

$$\begin{aligned}
 E_{n,\lambda} = & \left( n + \frac{1}{2} \right) + \frac{3}{4}\lambda(1 + 2n(n+1)) \\
 & - \lambda^2 \left( \frac{(n+1)(n+\frac{3}{2})^2(n+2)}{2 + 3\lambda(2n+3)} \right. \\
 & \quad \left. - \frac{n(n-\frac{1}{2})^2(n-1)}{2 + 3\lambda(2n-1)} \right. \\
 & \quad \left. + \frac{(n+1)(n+2)(n+3)(n+4)}{16(4 + 6\lambda(2n+5))} \right. \\
 & \quad \left. - \frac{n(n-1)(n-2)(n-3)}{16(4 + 6\lambda(2n-3))} \right) \quad (19)
 \end{aligned}$$

As can be seen in table III, the results agree for low  $\lambda$  but diverge as the contribution of the quartic factor increases, which is exactly the behavior we expected.

A comparative plot of the obtained data is reported in Figure 3. First, we take a look at the dependence on  $\lambda$  of the ground state and the state  $n = 2$  (Figures 3a and 3b). The general shape of the states remains the same, however as  $\lambda$  increases the state becomes more localized since the potential will grow more rapidly. Likewise, it is interesting to look at all the states for a given  $\lambda$  (Figures 3c, 3d). Once again they have the same general shape as the harmonic states, as expected.

### B. Oscillator with imaginary frequency

Lastly, setting an imaginary value for  $\omega$  or, equivalently, taking  $r = w^2 < 0$ , will allow us to study a potential that is used as a model for tunneling and bond formation in diatomic molecules.

Qualitatively, we can see from the shape of the potential that we can expect the ground state to be a bound state. Therefore, we set a negative value for  $E_{init}$  in the condition given in Eq.(11) to make it easier for the network to find negative energy states. For the potential parameters, we start with  $\lambda = 1$ ,  $w^2 = -14$ . Once the

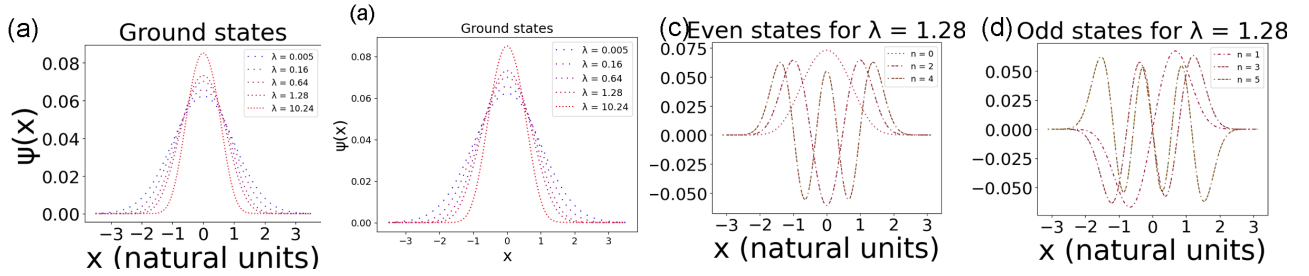


FIG. 3: (a) Ground state and (b) second excited state of the anharmonic oscillator for  $\omega = 1$ ;  $\lambda = 0.005, 0.16, 0.64, 1.28$ , and  $10.24$ . The color of the wave functions goes from blue to red as  $\lambda$  increases. (c) Even and (d) Odd stationary states of the anharmonic oscillator for  $\omega = 1$ ;  $\lambda = 1.28$ . The number of dashes between each dot in the plot corresponds to the value of  $n$  of that eigenstate

network has been trained for these parameters, we will be able to more easily find the solution for any other set of parameters by using transfer learning, as we did in the previous section.

For these given parameters, the energies of the two states are extremely close. As such, we had to impose a stricter convergence condition, stopping the training when the differential equation loss was less than  $2 \times 10^{-5}$ . Regardless, the network did converge for all the studied states and we obtained an energy estimate of  $-9.6808$  for the ground state and  $-9.6806$  for the first excited state. As expected, these energies are negative as they correspond to bound states. Furthermore, by increasing  $\lambda$  the eigenenergies get closer to 0, as the potential becomes closer to a pure quartic oscillator and, therefore, the states get closer to unbound states. It is also useful to look at the shape of these eigenstates (Figure 4). These are, once again, what we expect from the shape of the potential: two peaks corresponding to the minima in the potential. The ground and the first excited state are also extremely similar, except for one symmetric and one anti-symmetric, and the peak with the same sign almost perfectly overlaps, thus justifying the closeness of the energy levels. Lastly, it is interesting to note, from Figure 5a that the local minima of the wavefunction corresponding to  $x = 0$  assumes a higher value as  $\lambda$  increases. On the other hand, in the first excited we always have a node in  $x = 0$ , see Figure 5b.

## VI. PURE QUARTIC OSCILLATOR

We now relay the results for the pure quartic oscillator, i.e.

$$V(x) = \lambda x^4 \quad (20)$$

with  $\lambda = 1$ . In order to initialize the network to a good state, we start with the weights and biases of the anharmonic oscillator with  $\omega^2 = 1$  and  $\lambda = 1$ . The network converged effectively for all states. In Figure 6 we show one of the excited states of the pure quartic oscillator compared with the state at the same quantum number

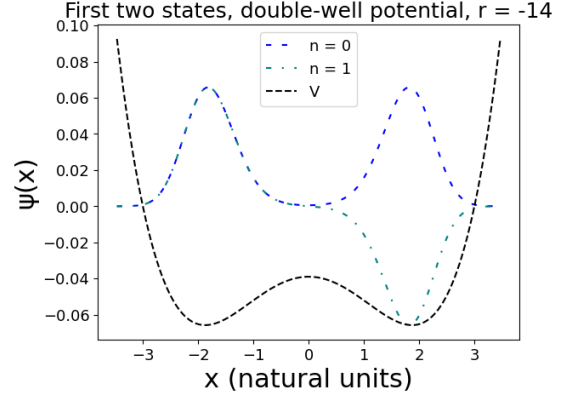


FIG. 4: Wave function for the ground state (blue sparse dashed line) and first excited state (blue-green dashed-dotted line) of the double-well. The potential (black dense dashed line) has been centered and scaled for better visualization, and should only be taken qualitatively

for the harmonic oscillator. Once again the two have the same general shape, but the quartic one is much more localized since the potential grows faster with the position  $x$ .

## VII. ENERGY BEHAVIOR

The last result of our paper concerns the scaling behavior and the spacing of the energy levels in function of  $\lambda$ . It is indeed interesting to check whether our method is able to assess the departure from the validity of the perturbative regime. We compare in Figure 7 the eigenvalues of the anharmonic oscillator against the ones of the pure quartic oscillator. It is easy to see how the eigenvalues of the pure quartic oscillator increase at a roughly exponential rate when plotted against the logarithm of  $\lambda$  (or, equivalently, they are proportional in log-log scale). On the other hand, we can recognize two regimes for the values of the anharmonic oscillator. Both seem to be roughly exponential, but for low values of  $\lambda$  the energy



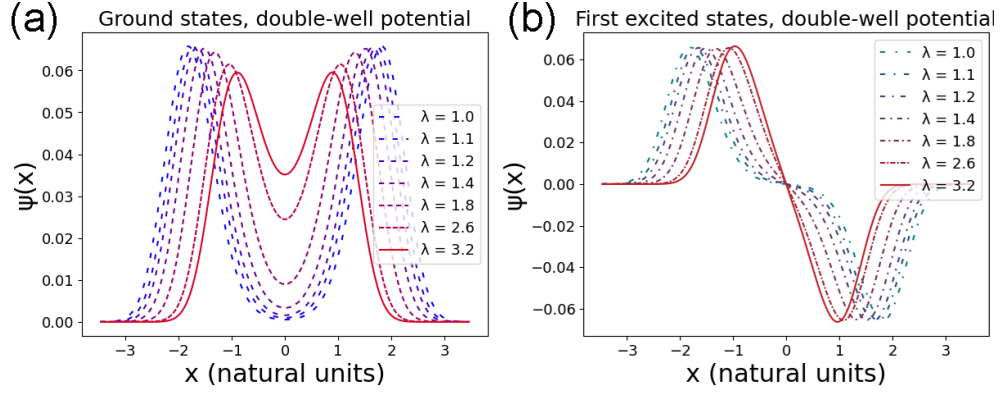


FIG. 5: (a) Ground state and (b) second excited state of the double-well for  $r = -14$ ;  $\lambda = \{1, 1.1, 1.2, 1.4, 1.8, 2.6, 3.2\}$ . The color of the wave functions goes from blue to red as  $\lambda$  increases. Furthermore, the spacing between each dash becomes tighter the higher  $\lambda$ .

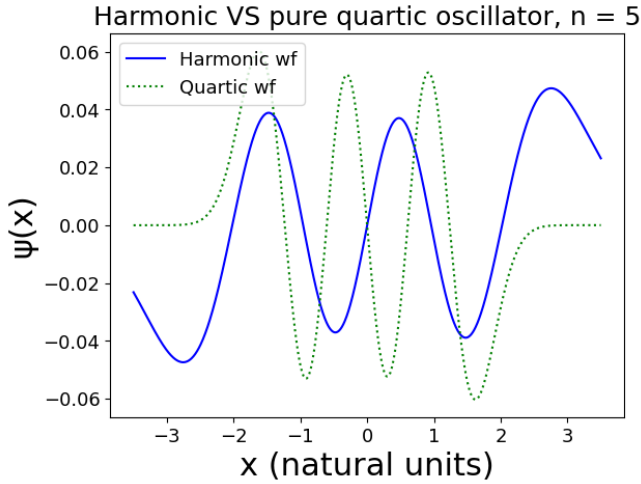


FIG. 6: Comparison between the fifth excited state of the harmonic oscillator (blue solid line) and the pure quartic oscillator (green dotted line).

increases much slower than for higher ones. Furthermore, for high  $\lambda$  the anharmonic and pure quartic eigenvalues line up, since the harmonic contribution becomes negligible. We can get a rough idea of this behavior by performing a linear fit for the logarithms of  $\lambda$  and  $E$ . In particular, we perform three fits: one for the low- $\lambda$  region (roughly  $\lambda < 0.1$ ) of the anharmonic oscillator, one for the high- $\lambda$  region (roughly  $\lambda > 2.0$ ) of the anharmonic oscillator, and lastly a fit for all the values of the quartic oscillator. We obtain, as expected, exponential behavior for each of the studied regions. Furthermore, we can see how the high- $\lambda$  behavior of the anharmonic oscillator matches the quartic oscillator for the last values of  $\lambda$  when the quadratic part becomes negligible. See Appendix A for the numerical values of the fits.

Considering the numerical analysis that we performed, a comment on the errors is in order. In our work there

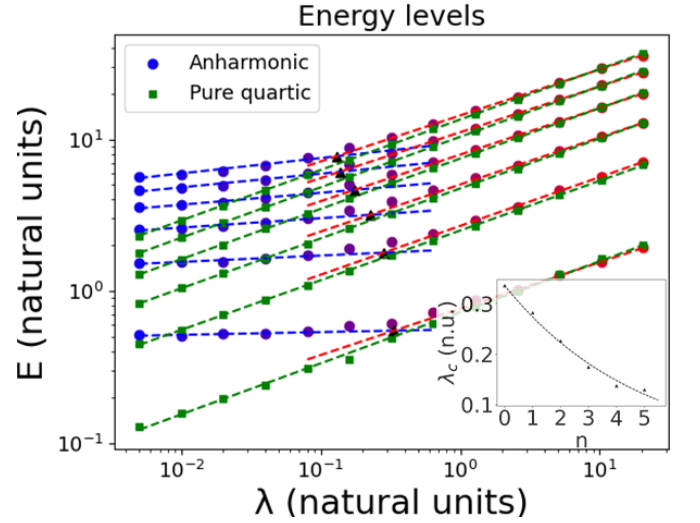


FIG. 7: Energy levels of the anharmonic oscillator (blue or red circles) in comparison with the pure quartic oscillator (green squares), with exponential fits for the anharmonic eigenvalues at low  $\lambda$  (blue dashed line), anharmonic eigenvalues at high  $\lambda$  (red dashed line), pure eigenvalues at high  $\lambda$  (green dashed line). Both axes are in logarithmic scale. In the inset: A plot showing the values of  $\lambda$  corresponding to the intersections of the two exponentials corresponding to the low- $\lambda$  and high- $\lambda$  regimes for each energy level ( $\lambda_c$ ).

On the horizontal axis is the quantum number  $n$ , whereas and on the vertical axis is  $\lambda_c$ . These values have also been fitted and show a roughly exponential behavior. The intersection points have also been signaled as black triangles in the main plot.

can be three major possible sources of uncertainty for the guess of the energy. The first is due to the stochasticity of the gradient descent. The second is due to the random initialization. We can estimate a lower bound for the magnitude of these two by running the training for the



ground state of the harmonic oscillator ten times, and then looking at the standard deviation of the guesses for the energy. We obtain a  $\sigma$  of 0.7% the value of the energy. The third is due to the choice of collocation points. Those are the ones that make up the uncertainty displayed in the results of Tables II and III

### VIII. CONCLUSIONS

In this work, we utilized a novel unsupervised deep-learning-based model to find the eigenvalues and eigenstates for a potential with a plethora of application in physics. To benchmark the performances of our method, we first started by finding the first six stationary states of the harmonic oscillator. The obtained results then served as initialization to solve the anharmonic oscillator and its pure quartic version for growing values of the parameter  $\lambda$ . Our method is reliable on the full range of  $\lambda$  and it allowed us to establish two exponential scalings for the energy levels. The result seems to suggest there is a critical value  $\lambda_c$  that decreases with the energy for which the perturbative expansion is not longer reliable. This is consistent with the previous results, in fact, the spectrum does not have a constant spacing due to its nonlinear dependence on the occupation number [14]. Therefore, this opens an interesting avenue of research to study if such conclusions can be drawn also for field theories in higher dimensions and in particular if this could be related to the phase transition that could be studied via mapping of the scalar  $\lambda\phi^4$  in  $(3+1)$ -dimensions to an Ising model in  $d \geq 4$  dimensions. For the machine learning side, since the changes in the wave function as  $\lambda$  increases seem to be smooth it is, in principle, possible to use these results to train a neural network that can take both  $\lambda$  and  $x$  as the input, and outputs the wave function at  $x$  and energy for a given eigenstate of the potential with the given  $\lambda$ .

#### Code Availability

The code producing the results in the paper is available upon reasonable request from the Authors.

#### Acknowledgements

The Authors acknowledge the project CQES of the Italian Space Agency (ASI) for having partially supported this research (grant N. 2023-46-HH.0).

#### Author contribution statement

L.B. and A.M. contributed equally to this work.

### Appendix A: Coefficients of the linear fits

In this Section we report the numerical coefficients of the fits in Figure 7. In Table IV we report the interpolation coefficients used to draw the blue dashed lines in Figure 7, equivalently in Tables V and VI we report the interpolation coefficients used to draw the red and green dashed lines in Figure 7. That is, the coefficients of the line:

$$\log(E_n) = a \log(\lambda) + b \quad (\text{A1})$$

We can see, in particular, that the values of  $a$  for the low- $\lambda$  region ( $\lambda < 0.1$ ) are much lower than for the other two. On the other hand, the high- $\lambda$  ( $\lambda > 2$ ) and quartic coefficients are comparable. We expect that if we were to redo the fit with higher values of  $\lambda$  and increase the cutoff for the high- $\lambda$  region each of the pairs at the same  $n$  will become increasingly similar. At any rate, we can say that in each of the three cases  $\log(\lambda)$  and  $\log(E)$  are directly proportional.

In Table VII we show the values  $\lambda_c$  of  $\lambda$  for which the low- $\lambda$  and high- $\lambda$  fits intersect and the corresponding energies  $E_c$ , which can be used as an indication for the phase transition from the low- $\lambda$  perturbative regime to the high- $\lambda$  quartic regime. The critical value  $\log(\lambda_c)$  seems to be inversely proportional with respect to the  $n$ -th energy level,  $\lambda_c$  decreases as the energy of the state increases, causing an earlier deviation from the perturbative regime.

n	a	b
0	0.0180	-0.580
1	0.0419	0.635
2	0.0621	1.25
3	0.0787	1.67
4	0.0903	1.99
5	0.101	2.25

TABLE IV: The fit coefficients for the  $\lambda < 0.1$  region, anharmonic oscillator

n	a	b
0	0.305	-0.266
1	0.321	0.989
2	0.310	1.62
3	0.307	2.07
4	0.302	2.41
5	0.303	2.66

TABLE V: The fit coefficients for the  $\lambda > 2$  region, anharmonic oscillator

n	a	b
0	0.336	-0.321
1	0.327	0.919
2	0.329	1.56
3	0.332	2.01
4	0.332	2.34
5	0.332	2.60

TABLE VI: The fit coefficients for the interpolation lines plot of the pure quartic oscillator

n	$\lambda_c$	$E_c$
0	0.333	0.549
1	0.282	1.79
2	0.226	3.18
3	0.175	4.64
4	0.137	6.11
5	0.129	7.72

TABLE VII: The fit coefficients for the pure quartic oscillator

- 
- [1] A. Altland and B. D. Simons, *Condensed Matter Field Theory*, 2nd ed. (Cambridge University Press, 2010).
- [2] S. Coleman, B. Chen, and D. Kaiser, *Quantum Field Theory: Lectures of Sidney Coleman*, G - Reference, Information and Interdisciplinary Subjects Series (World Scientific, 2019).
- [3] R. J. Glauber, Nobel lecture: One hundred years of light quanta, *Rev. Mod. Phys.* **78**, 1267 (2006).
- [4] S. Haroche, Nobel lecture: Controlling photons in a box and exploring the quantum to classical boundary, *Rev. Mod. Phys.* **85**, 1083 (2013).
- [5] W. H. Shaffer, Degenerate modes of vibration and perturbations in polyatomic molecules, *Rev. Mod. Phys.* **16**, 245 (1944).
- [6] N. Ashcroft and N. Mermin, *Solid State Physics* (Cengage, 2021).
- [7] A. V. Turbiner and J. C. del Valle Rosales, *Quantum Anharmonic Oscillator* (WORLD SCIENTIFIC, 2023) <https://www.worldscientific.com/doi/pdf/10.1142/13252>.
- [8] J. W. S. B. Rayleigh, *The theory of sound*, Vol. 2 (Macmillan, 1896).
- [9] E. Schrödinger, Quantisierung als eigenwertproblem, *Annalen der Physik* **385**, 437 (1926).
- [10] C. M. Bender and T. T. Wu, Anharmonic oscillator, *Phys. Rev.* **184**, 1231 (1969).
- [11] C. M. Bender and T. T. Wu, Anharmonic oscillator. II. a study of perturbation theory in large order, *Phys. Rev. D* **7**, 1620 (1973).
- [12] C. M. Bender and T. T. Wu, Analytic structure of energy levels in a field-theory model, *Phys. Rev. Lett.* **21**, 406 (1968).
- [13] Y. Guo and W. Li, Solving anharmonic oscillator with null states: Hamiltonian bootstrap and Dyson-Schwinger equations, *Phys. Rev. D* **108**, 125002 (2023).
- [14] R. Maxton and Y. Meurice, Perturbative boundaries of quantum advantage: Real-time evolution for digitized  $\lambda\phi^4$  lattice models, *Phys. Rev. D* **107**, 074508 (2023).
- [15] W. Li, Principle of minimal singularity for Green's functions, *Phys. Rev. D* **109**, 045012 (2024).
- [16] Y. Hatsuda and M. Kimura, Perturbative quasinormal mode frequencies, *Phys. Rev. D* **109**, 044026 (2024).
- [17] N. R. Werthamer, Self-consistent phonon formulation of anharmonic lattice dynamics, *Phys. Rev. B* **1**, 572 (1970).
- [18] P. Shih and T. C. Berkelbach, Anharmonic lattice dynamics from vibrational dynamical mean-field theory, *Phys. Rev. B* **106**, 144307 (2022).
- [19] T. Tadano and S. Tsuneyuki, Quartic anharmonicity of rattlers and its effect on lattice thermal conductivity of clathrates from first principles, *Phys. Rev. Lett.* **120**, 105901 (2018).
- [20] B. Temelso and G. C. Shields, The role of anharmonicity in hydrogen-bonded systems: The case of water clusters, *Journal of Chemical Theory and Computation* **7**, 2804 (2011).
- [21] Y. Harabuchi, R. Tani, N. De Silva, B. Njegic, M. S. Gordon, and T. Taketsugu, Anharmonic vibrational computations with a quartic force field for curvilinear coordinates, *The Journal of Chemical Physics* **151**, 064104 (2019).
- [22] I. Bialynicki-Birula and J. Mycielski, Nonlinear wave mechanics, *Annals of Physics* **100**, 62 (1976).
- [23] H. Dekker, Classical and quantum mechanics of the damped harmonic oscillator, *Physics Reports* **80**, 1 (1981).

- [24] L. Domingo, J. Borondo, and F. Borondo, Using reservoir computing to construct scarred wave functions, *Phys. Rev. E* **109**, 044214 (2024).
- [25] Z. T. Wang, Y. Ashida, and M. Ueda, Deep reinforcement learning control of quantum cartpoles, *Phys. Rev. Lett.* **125**, 100401 (2020).
- [26] M. Maronese, C. Destri, and E. Prati, Quantum activation functions for quantum neural networks, *Quantum Information Processing* **21**, 128 (2022).
- [27] L. Moro and E. Prati, Anomaly detection speed-up by quantum restricted boltzmann machines, *Communications Physics* **6**, 269 (2023).
- [28] S. Corli, D. Dragoni, M. Proietti, M. Dispenza, C. Cavazzoni, and E. Prati, A max k-cut implementation for qaoa in the measurement based quantum computing formalism, in *2023 IEEE International Conference on Quantum Computing and Engineering (QCE)*, Vol. 2 (IEEE, 2023) pp. 284–285.
- [29] L. Rocutto, C. Destri, and E. Prati, Quantum semantic learning by reverse annealing of an adiabatic quantum computer, *Advanced Quantum Technologies* **4**, 2000133 (2021).
- [30] M. Lazzarin, D. E. Galli, and E. Prati, Multi-class quantum classifiers with tensor network circuits for quantum phase recognition, *Physics Letters A* **434**, 128056 (2022).
- [31] M. Grossi, O. Kiss, F. De Luca, C. Zollo, I. Gremese, and A. Mandarino, Finite-size criticality in fully connected spin models on superconducting quantum hardware, *Phys. Rev. E* **107**, 024113 (2023).
- [32] S. Monaco, O. Kiss, A. Mandarino, S. Vallecorsa, and M. Grossi, Quantum phase detection generalization from marginal quantum neural network models, *Phys. Rev. B* **107**, L081105 (2023).
- [33] H. Jin, M. Mattheakis, and P. Protopapas, Physics-informed neural networks for quantum eigenvalue problems (2022), arXiv:2203.00451 [cs.LG].
- [34] L. Harcombe and Q. Deng, Physics-informed neural networks for discovering localised eigenstates in disordered media (2023), arXiv:2305.06802 [cond-mat.dis-nn].
- [35] L. Yuan, Y.-Q. Ni, X.-Y. Deng, and S. Hao, A-pinn: Auxiliary physics informed neural networks for forward and inverse problems of nonlinear integro-differential equations, *Journal of Computational Physics* **462**, 111260 (2022).
- [36] M. Raissi, P. Perdikaris, and G. Karniadakis, Physics-informed neural networks: A deep learning framework for solving forward and inverse problems involving nonlinear partial differential equations, *Journal of Computational Physics* **378**, 686 (2019).
- [37] X. I. A. Yang, S. Zafar, J.-X. Wang, and H. Xiao, Predictive large-eddy-simulation wall modeling via physics-informed neural networks, *Phys. Rev. Fluids* **4**, 034602 (2019).
- [38] M. Raissi, A. Yazdani, and G. E. Karniadakis, Hidden fluid mechanics: Learning velocity and pressure fields from flow visualizations, *Science* **367**, 1026 – 1030 (2020).
- [39] B. Reyes, A. A. Howard, P. Perdikaris, and A. M. Tarkovsky, Learning unknown physics of non-newtonian fluids, *Phys. Rev. Fluids* **6**, 073301 (2021).
- [40] S. Cai, Z. Wang, S. Wang, P. Perdikaris, and G. E. Karniadakis, Physics-informed neural networks for heat transfer problems, *Journal of Heat Transfer* **143**, 10.1115/1.4050542 (2021), cited by: 338.
- [41] Y. Chen, L. Lu, G. E. Karniadakis, and L. D. Negro, Physics-informed neural networks for inverse problems in nano-optics and metamaterials, *Optics Express* **28**, 11618 – 11633 (2020).
- [42] R. Luna, J. Calderón Bustillo, J. J. Seoane Martínez, A. Torres-Forné, and J. A. Font, Solving the Teukolsky equation with physics-informed neural networks, *Phys. Rev. D* **107**, 064025 (2023).
- [43] S. Qiu, S. Han, X. Ju, B. Nachman, and H. Wang, Holistic approach to predicting top quark kinematic properties with the covariant particle transformer, *Phys. Rev. D* **107**, 114029 (2023).
- [44] M. Tsubaki and T. Mizoguchi, Quantum deep field: Data-driven wave function, electron density generation, and atomization energy prediction and extrapolation with machine learning, *Phys. Rev. Lett.* **125**, 206401 (2020).
- [45] E. Brézin, J. C. Le Guillou, and J. Zinn-Justin, Perturbation theory at large order. I. the  $\varphi^{2N}$  interaction, *Phys. Rev. D* **15**, 1544 (1977).
- [46] R. Seznec and J. Zinn-Justin, Summation of divergent series by order dependent mappings: Application to the anharmonic oscillator and critical exponents in field theory, *Journal of Mathematical Physics* **20**, 1398 (1979).
- [47] J. Zinn-Justin, Expansion around instantons in quantum mechanics, *Journal of Mathematical Physics* **22**, 511 (1981).
- [48] J. Zinn-Justin, Perturbation series at large orders in quantum mechanics and field theories: Application to the problem of resummation, *Physics Reports* **70**, 109 (1981).
- [49] A. V. Turbiner and J. C. del Valle, Anharmonic oscillator: a solution, *Journal of Physics A: Mathematical and Theoretical* **54**, 295204 (2021).
- [50] M. Bina, A. Mandarino, S. Olivares, and M. G. A. Paris, Drawbacks of the use of fidelity to assess quantum resources, *Phys. Rev. A* **89**, 012305 (2014).
- [51] A. Mandarino, M. Bina, S. Olivares, and M. G. Paris, About the use of fidelity in continuous variable systems, *International Journal of Quantum Information* **12**, 1461015 (2014).
- [52] A. Mandarino, M. Bina, C. Porto, S. Cialdi, S. Olivares, and M. G. A. Paris, Assessing the significance of fidelity as a figure of merit in quantum state reconstruction of discrete and continuous-variable systems, *Phys. Rev. A* **93**, 062118 (2016).
- [53] F. Hioe, D. MacMillen, and E. Montroll, Quantum theory of anharmonic oscillators. II. energy levels of oscillators with  $x^{2\alpha}$  anharmonicity, *Journal of Mathematical Physics* **17**, 1320 (1976).